Research Article Vol. 4, No. 5 / 15 May 2025 / Optics Continuum 1147
OPTICS CONTINUUM

Spectral shaping of a broadband multimode diode laser using a virtually imaged phased array

MANUEL ALEJANDRO LEFRÁN TORRES,[1,†,*] DAVID RODRÍGUEZ FERNÁNDEZ,[1,†] JAIME JAVIER BORGES MARQUEZ,[1,†] MARCIO HERACLYTO GONÇALVES DE MIRANDA,[2,†] NADIA BOULOUFA-MAAFA,[3,†] AND LUIS GUSTAVO MARCASSA[1,†]

[1]*Instituto de Física de São Carlos, Universidade de São Paulo, Avenida Trabalhador São-Carlense, São Carlos, 13566-590 São Paulo, Brazil*
[2]*Departamento de Física, Universidade Federal de Pernambuco, Av. Professor Luiz Freire, Recife, 50670-901 Pernambuco, Brazil*
[3]*Université Paris-Saclay, CNRS, Laboratoire Aimé Cotton, 91400, Orsay, France*
[†]These authors contributed equally to this work.
[*]*lefran@ifsc.usp.br*

Abstract: We have built a spectral shaping system, based on a virtually imaged phased array (VIPA) and a digital micromirror device (DMD), to manipulate a multimode diode laser spectrum. Due to its working principles, the system reduces the available optical power by ~ −27 dB. To overcome this limitation, we have seeded its output, using a double-pass configuration, in a tapered amplifier, to increase the available power to ~ 60 mW. We have implemented spectral features with a resolution of 0.1 cm^{-1}, which is limited by the characterization spectrometer. This may be attractive for a wide range of applications, especially for cooling the translational, vibrational, and rotational degrees of freedom of a diatomic molecule.

1. Introduction

Broadband laser sources are fundamental tools for molecular spectroscopy since the first lasers were created [1]. For complex molecules, the number of rovibrational energy levels in a large spectral width gets higher, presenting a forest of spectral lines, sometimes hard to resolve. For this matter, high-resolution broadband sources are required. Lately, broadband laser sources, such as frequency combs, superluminescent diodes, and frequency-shifted feedback lasers (FSF), are commonly used for applications like direct frequency comb spectroscopy [2], trace detection of molecules [3], loading ultracold molecules in the ground state [4], pumping He* gas at room temperature [5]. Furthermore, it has been suggested that FSF lasers could be applied to the formation of cold molecules [6]. The control of rovibrational levels is fundamental for the production of dense and cold molecular samples.

Rovibrational optical pumping of cold molecules has been an intense research field [4,7–9]. However, the molecular rotational constant is small, and a precise spectral shaping is necessary. For example, the rotational constant of the ground potential $X^1\Sigma_g^+$ in the Rb_2 molecule is around ~0.022 cm^{-1}. Cournol et al [10] suggested that it could be achieved using a virtually imaged phased array (VIPA) [11,12]. Recently, it has been proposed that spectrally shaped broadband laser sources, using a VIPA, could be responsible for rovibrational as well as translational cooling

#559281 https://doi.org/10.1364/OPTCON.559281
Journal © 2025 Received 11 Feb 2025; revised 14 Apr 2025; accepted 16 Apr 2025; published 13 May 2025

OPTICS CONTINUUM

of the Rb_2 molecule [13]. In this article, we have built a spectral shaping system, based on a VIPA and a digital micromirror device (DMD), to manipulate a multimode diode laser spectrum. We have characterized the system using a single frequency laser, demonstrating a spectral resolution of 0.02 cm^{-1}. However, the available power was reduced by approximately ∼−27 dB. Therefore, it was necessary to seed the system using a double-pass configuration in a tapered amplifier (TA) to increase the power to ∼ 60 mW. We have demonstrated that the TA output can be manipulated with a resolution of 0.1 cm^{-1}. In the following, we first present our experimental setup and then present the spectral properties of the system.

2. Experimental setup

A key element in the experimental system is the VIPA, which is a Fabry-Perot etalon consisting of two parallel flat mirrors separated by a distance t [11,12] (Fig. 1). The first surface, the incident surface, has a reflectivity of approximately 100%, except for a window intended for optical access of the light beam, which features an anti-reflective coating. The second transmission surface is coated with a film with a reflectivity greater than 95%. The space between the mirrors is filled with either glass or air. The incident laser beam is coupled into the access window with the aid of a cylindrical lens, forming an angle θ, small in relation to the perpendicular direction of the VIPA. After the beam reflects off the second surface, a small amount is transmitted through the VIPA, while the majority is reflected. Then, the beam is reflected by the first surface, and the optical path difference between these two reflections is given by $d = 2t\cos\theta$. Successive reflections generate virtual sources separated by d. In summary, the incident light is dispersed by the VIPA at an angle (ϕ) that depends on the phase difference between the virtual images, i.e., the frequency of the radiation, the angle of incidence, and the thickness of the VIPA. An important characteristic of the VIPA is that frequencies separated by an integer number of the free spectral range (FSR) will be dispersed to the same spatial positions.

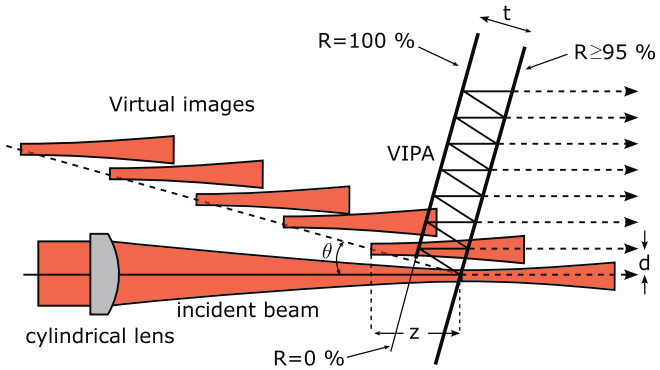

Fig. 1. Experimental setup. Scheme of the VIPA. The incident beam is coupled with the help of a cylindrical lens. The numerous reflections generate virtual images.

Therefore, when the bandwidth of the light sources is greater than the free spectral range (FSR), there will be an overlap of frequencies for each spatial position where the light is dispersed, separated by an integer multiple of the FSR. Thus, it is necessary to break this frequency degeneracy. To address this issue, a pulse shaper described in the literature is employed, which uses a transmission grating to break the spatial degeneracy of the VIPA, allowing access to very fine resolution across a wide spectrum range [14,15]. Although this dispersion scheme has been reported in prior applications such as frequency comb spectroscopy [16], optical communications [17], polarization sensing [18], and pulse shaping [19], it has never been implemented in a

OPTICS CONTINUUM

continuous multimode diode laser pulse shaper. This implementation is of great importance in the rotational optical pumping of molecules [13].

The first part of our experimental setup is the spectral shaping system (Fig. 2). We start from a multimode diode laser (MMDL) (RPMC, LDX-3230-680) operating at ~ 682 nm, with a total power of 1.5 W, which is collimated using a combination of spherical and cylindrical lenses. The laser spectrum typically exhibits peaks spaced by ~0.8 cm^{-1}. An optical isolator (OI) guarantees that no reflection, from the spectral shaping system, feedbacks into the laser. A cylindrical lens (CL1, focal length 10 cm) focuses the laser beam onto the VIPA in the vertical direction. The VIPA is manufactured by LightMachinery (model OP-6721-6743-3), operating in the 600-725 nm range with a free spectral range of 15 GHz (0.5 cm^{-1}) and a typical finesse of ~ 70. A cylindrical lens telescope (CL2, focal length 5 cm and CL3, focal length 25 cm) expands the laser beam in the horizontal direction, illuminating 5 cm of a 2400 groves/mm holographic diffraction grating (G). It is important to note that the resolution of the grating must be sufficient to separate two frequencies separated by the VIPA free spectral range, breaking its degeneracy. The first-order diffraction beam passed through two cylindrical lenses (CL4, focal length 70 cm and CL5, focal length 50 cm). CL4 is parallel to the VIPA direction, and CL5 is parallel to the diffraction grating direction. Both lenses focus the beam onto the same Fourier plane. Figure 3 shows the multimode diode laser profile at the Fourier plane using a laser beam profiler (Newport, LBP-1-USB). The VIPA dispersion occurs along the y direction, while the grating dispersion occurs along the x direction. The different frequency modes are spatially separated, two adjacent spots in the y direction are separated by the VIPA spectral resolution within the FSR. While frequencies separated by an integer number of FSR are resolved by the grating in the x direction. To shape the spectrum, the digital micromirror device (DMD, Vialux, model V-9001 2560 × 1600 pixels) is placed at the Fourier plane, and its reflection counterpropagates the incident beam, emerging at the polarizing beam splitter (PBS1). The available power after the shaping system (without spectral mask) was reduced by approximately ~−27 dB, with losses of about ~16 dB in the VIPA, around ~6 dB in the diffraction grating, approximately ~4 dB in the DMD, and ~1 dB in the optics. The losses in the diffraction grating and DMD are within the expected range. However, the loss in the VIPA is higher than the ~12 dB reported in the literature for a single-mode Gaussian laser [14]. This discrepancy is attributed to the fact that our laser operates with multiple longitudinal and transverse modes, resulting in significantly higher losses compared to a single-mode laser. The total power after the shaping system (about 3 mW), without any spectral shaping, is not enough for atomic physics applications. To amplify it, we incorporated an amplification system into our setup. In this assembly, we perform a double pass through a 250 mW tapered amplifier (TA) (EagleYard, EYP-TPA-0670-00250) before directing it to a homemade grating spectrometer via a single-mode fiber. The fiber output passes through a cylindrical telescope, illuminating 5 cm of a 2400 grooves/mm holographic diffraction grating. The first-order diffraction is focused by a spherical mirror (focus 1 m) onto a CCD camera (Thorlabs, DCC1545M). A single-frequency diode laser (TOPTICA, model DL pro), operating at 682 nm and monitored by a wavemeter (HighFinesse, model WS7), is utilized to calibrate both the spectral shaping system and the homemade grating spectrometer, with a resolution of 0.1 cm^{-1}. The Fig. 4 shows a scheme of the complete experimental setup.

OPTICS CONTINUUM

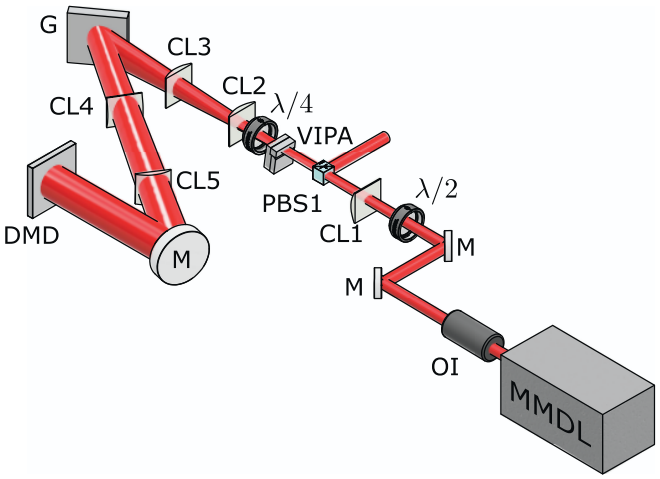

Fig. 2. Spectral shaping setup. The system is composed of: multimode diode laser (MMDL), optical isolators (OI), waveplates ($\lambda/2$ and $\lambda/4$), polarizing beamsplitter (PBS), cylindrical lenses (CL), virtual imaging phase array (VIPA), diffraction grating (G), digital micromirror device (DMD) and mirrors (M).

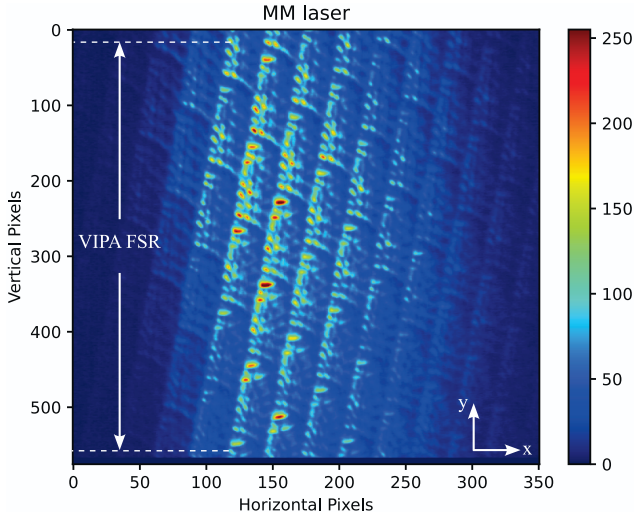

Fig. 3. Multimode diode laser profile at the Fourier plane in a laser beam profiler. The different frequency modes are spatially separated in tilted lines. This lines are a product of the dispersion from the VIPA (vertical direction) and the diffraction grating (horizontal direction).

OPTICS CONTINUUM

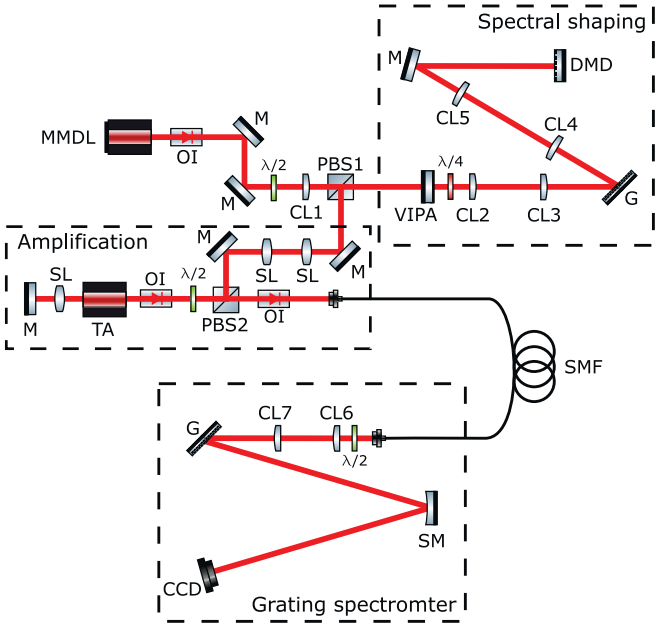

Fig. 4. Experimental setup. The whole system is composed of: multimode diode laser (MMDL), optical isolators (OI), waveplates ($\lambda/2$ and $\lambda/4$), polarizing beamsplitters (PBS), cylindrical lenses (CL), virtual imaging phase array (VIPA), diffraction grating (G), digital micromirror device (DMD), mirrors (M), spherical mirror (SM) and CCD camera (CCD).

3. Results

3.1. Spectral shaping system characterization

Initially, we have characterized the optical properties of the spectral shaping system. To do this, first we have replaced the multimode diode laser with the single frequency laser, and the DMD by the laser beam profiler (Newport, LBP-1-USB), which was placed on a 12 mm travel DC servomotor actuator, controlled by the Thorlabs KDC101 DC servomotor controller. The position of the LBP was adjusted to minimize the laser spot, finding the Fourier plane. This procedure allows us to measure the waist of the laser beam in both the vertical and horizontal directions. Measurements were taken by identifying the points where the intensity of the beam had decreased to 13.5% (approximately e^{-2}) of its maximum value. The size of the waist in the vertical direction was approximately 150 μm, while in the horizontal direction it was around 40 μm. Considering the DMD's pixel size of 7.6×7.6 μm, the laser size corresponds to 20 pixels vertically by 5 pixels horizontally in the Fourier plane. The beam waist is larger in the vertical direction compared to the horizontal direction, due to the VIPA's greater dispersion angle in contrast to the diffraction grating. Figure 5(a) shows the LBP image for two different frequencies separated by 0.02 cm^{-1} in the VIPA direction. Figure 5(b) shows the laser beam vertical profile. These figures show that the spectral resolution is better than 0.02 cm^{-1}. Figure 5(c) shows the LBP image for two different frequencies separated by 0.5 cm^{-1} in the diffraction grating direction. Figure 5(d) shows the laser beam horizontal profile. These figures show that the diffraction grating breaks the degeneracy of the VIPA, allowing the system bandwidth to be greater than the VIPA's free spectral range (FSR). Such results agree with VIPA finesse and the resolving power of the grating.

In the next step, it was necessary to place the DMD at the Fourier plane to obtain the single frequency beam exiting at PBS1, therefore, the LBP was replaced by the DMD in the travel DC

OPTICS CONTINUUM

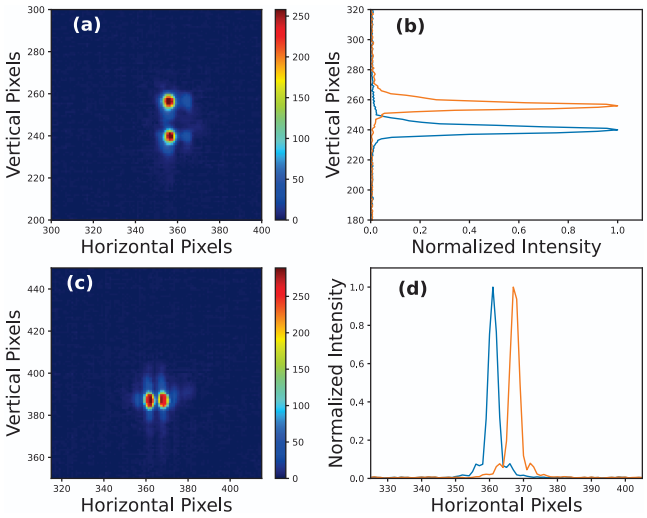

Fig. 5. a) LBP image at the Fourier plane for two different frequencies separated by 0.02 cm^{-1} in the VIPA direction. b) Laser beam vertical profile. c) LPB image at the Fourier plane for two different frequencies separated by 0.5 cm^{-1} in the diffraction grating direction. d) Laser beam horizontal profile.

servo motor actuator. Then, we activated a super pixel of 5×20 pixels on the DMD, which size was previously measured by the LPB. We found the laser frequency at this superpixel position by scanning its frequency and monitoring the power at the output of PSB1. Subsequently, we scanned the position of the DMD to maximize the power at the output of PSB1. The position at which the power is maximized is the position where the laser is fully focused on the superpixel, thus indicating the Fourier plane position. This whole process was automated using Python. Next, we turned on the 5×20 superpixel again and scanned the laser while monitoring the power at the output of PSB1. Figure 6 shows this output as a function of the laser frequency (red line), with a linewidth of about 0.02 cm^{-1}. It is possible to observe small transmission peaks ($\sim 2\%$), separated by the VIPA free spectral range, which are due to the diffraction of the laser beam on the DMD structure. In the following, the DMD was programmed to reflect frequencies below 14606.87 cm^{-1} only (black line Fig. 6). Again, due to diffraction on the DMD, it is possible to observe a small transmission of higher frequencies. These characterizations allowed us to demonstrate that the spectral shaping system has a resolution of 0.02 cm^{-1}.

3.2. *Tapered amplifier spectra*

In next step, we have replaced the single frequency laser by the multimode diode laser, and obtained its full spectrum at the exit of PBS1. Although we have characterized the spectral shaping system using a single frequency laser, such a laser cannot be used to spectrally calibrate de DMD for the multimode diode laser, because the lasers have different spatial modes. In principle, such calibration could be obtained by measuring the spectrum for each “superpixel" using the homemade grating spectrometer. The multimode diode laser has a linewidth of $\Delta\nu_{MMDL} \sim 20\, cm^{-1}$. In the direction of the VIPA (vertical), the MMLD illuminates almost the entire DMD due to the different dispersion orders of the VIPA. In the direction of the grating, since only the first diffraction order is utilized, we have a discrete number of vertically separated columns, spectrally spaced by the FSR ($\Delta\nu_{FSR} = 0.5\ cm^{-1}$). Since $\Delta\nu_{MMDL}/\Delta\nu_{FSR} = 40$, this means that we would have 40 vertical columns, each with a dimension of 5×1600 pixels. In the horizontal direction, we would have 80 rows of 2560×20. By multiplying the number of rows

OPTICS CONTINUUM

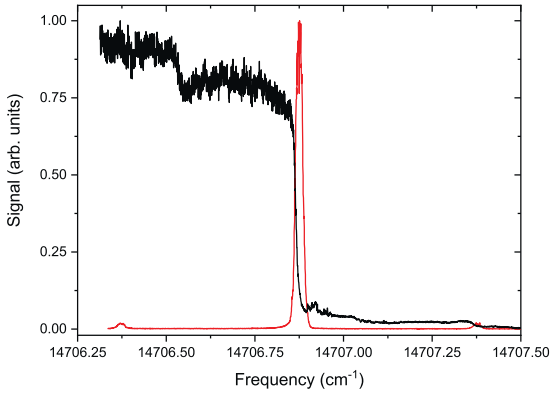

Fig. 6. Single frequency laser power at the PBS1 as a function of the laser frequency. Initially, the DMD was programmed to reflect only one frequency (red line spectrum). The small transmission peaks, separated by the VIPA free spectral range, are due to the diffraction of the laser beam on the DMD structure. In the following, the DMD was programmed to reflect frequencies below 14606.87 cm^{-1} only (black line).

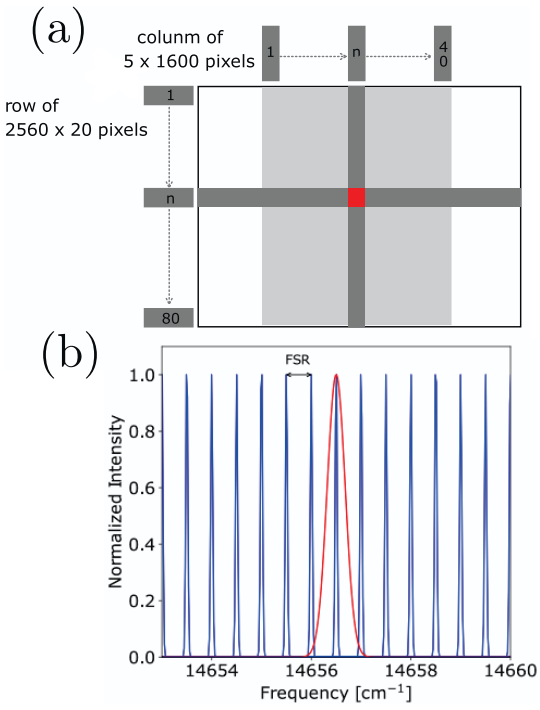

Fig. 7. a) Calibration technique of the DMD, the gray lines indicate the horizontal rows (20 pixels) and columns (5 pixels) where the DMD pixels are activated. First, all rows are stepped through, and then the main 40 columns. b) Simulated spectra of a row (blue line) and column (red line). The two spectra are multiplied to determine the wavelength in the superpixel (red).

OPTICS CONTINUUM

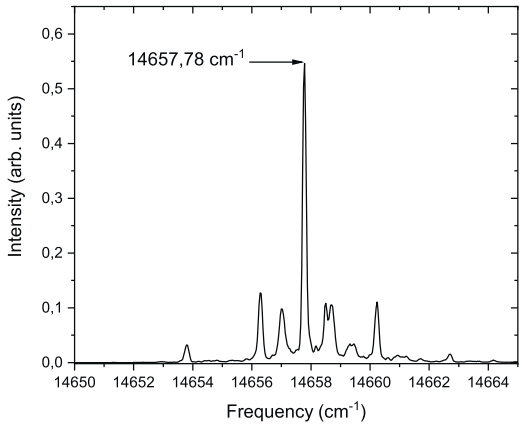

Fig. 8. Experimental result obtained by multiplying the spectrum of the row located at pixel 460 by the column located at pixel 2040. Thus, the superpixel located at this position is assigned the frequency of 14657.78 cm^{-1}.

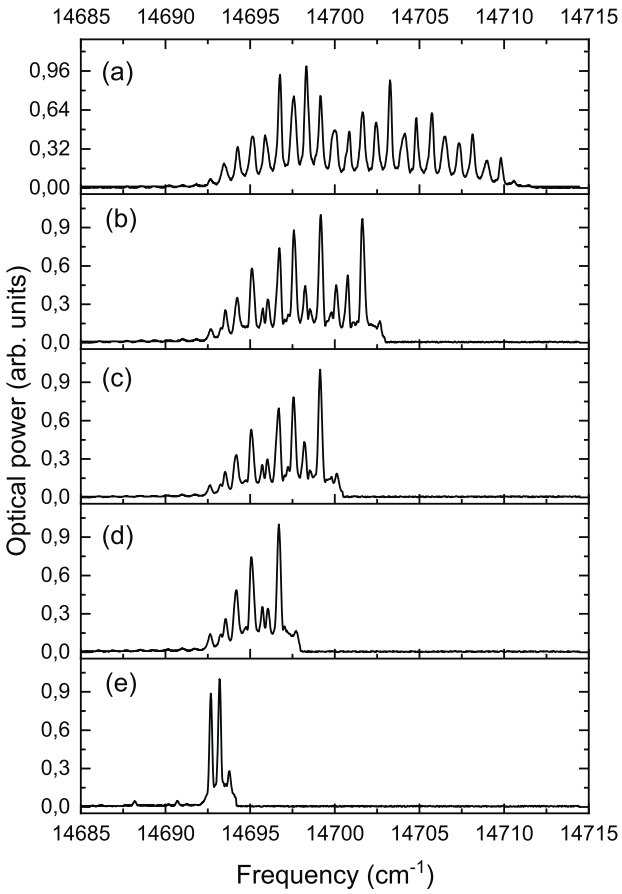

Fig. 9. Amplified laser beam spectra after the tapered amplifier, which was operating at 900 mA; (a) without the spectral mask and (b), (c), (d) and (e) with several different DMD masks.

OPTICS CONTINUUM

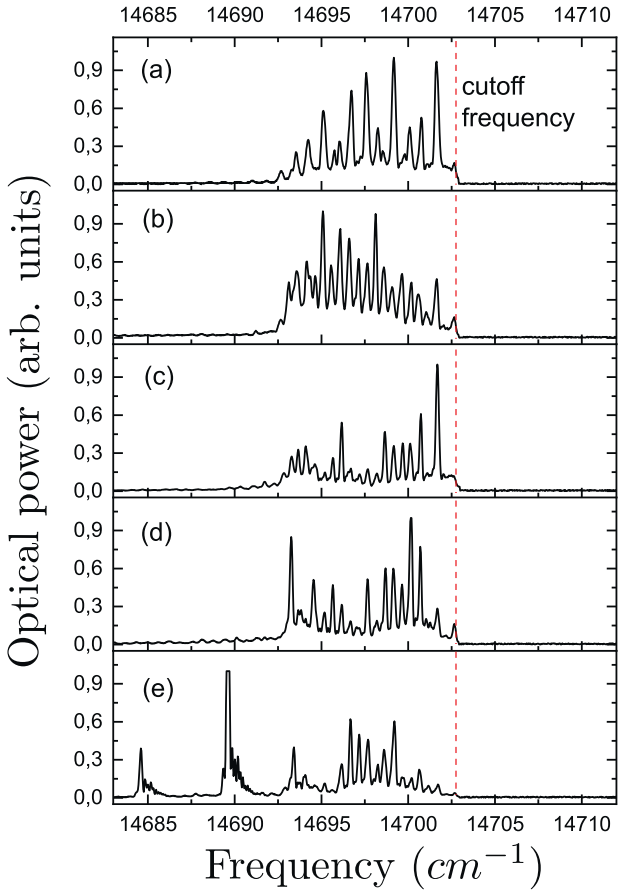

Fig. 10. Amplified laser beam spectra after the tapered amplifier as a function of its current. (a) shows the seed spectrum. (b) shows the spectrum at 800 mA.(c) shows the spectrum at 900 mA. (d) shows the spectrum at 1000 mA. (e) shows the spectrum at 1100 mA. At the maximum current, the TA feedbacks itself.

by the number of columns, we would obtain 3200 superpixels of 5×20. If each spectrum took about 30 seconds, the entire process would take more than 26 hours, which is not practical.

To overcome this limitation, we have applied a procedure developed by A. Metcalf and co-workers [19]. Figure 7 explains the basic idea behind the technique. In Fig. 7(a), the gray bars represent where the DMD pixels will be activated to reflect the whole spectrum of the MMDL. First, the DMD software sweeps through all 40 adjacent columns of dimensions 5×1600 pixels, recording the spectrum reflected by each column. Then it repeats the same process for all 80 rows of dimensions 2560×20 pixels. The data of the rows consist of several peaks separated by the FSR of the VIPA, corresponding to the blue trace in Fig. 7(b). However, the columns would provide a single peak, represented by the red trace in Fig. 7(b), with a width of ~FSR, as this is the maximum width that the VIPA can disperse. The recorded spectrum of the row is multiplied by the spectrum of the column to determine the exact wavelength position at each superpixel location, representing the intersection between them. For example, the red square shown in Fig. 7(a) provides the spatial location corresponding to the wavelength obtained by multiplying the spectrum of column N by the spectrum of row M. This calibration procedure requires the acquisition of 120 spectra, with an estimated time of one hour.

OPTICS CONTINUUM

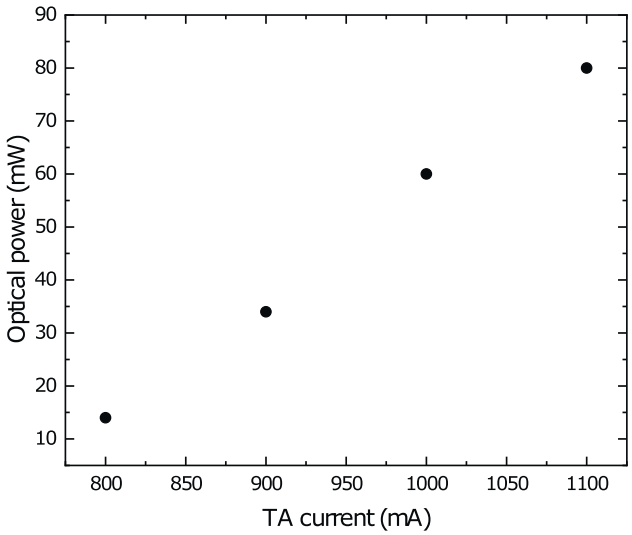

Fig. 11. Optical power as a function of the TA current.

Figure 8 shows an example of the experimental result obtained by multiplying the spectrum of the row located at pixel 460 by the column located at pixel 2040. Thus, the superpixel located at this position is assigned a frequency of 14657.78 cm^{-1}. After mapping, it is easy to program a mask on the DMD to perform a spectral cutoff at a specific frequency.

Figure 9 shows the amplified laser beam spectra after the tapered amplifier, which was operating at 900 mA, without any spectral mask (Fig. 9(a)) and with several different DMD masks (Fig. 9(b), (c), (d) and (e)). Clearly, we were able to cut the spectra very precisely at different frequencies, reducing the bandwidth from 20 to 2 cm^{-1}, without losing any optical power. This is the main advantage of using the TA in double-pass configuration [20]. This occurs because, during the first pass, the TA saturates with very low power, as demonstrated in Ref. [20]. We should point out that different spectra can be produced, with several regions within the multimode diode laser gain curve. We did not observe any temperature-related instability during the time period in which the experiments were conducted (5–6 hours).

Figure 10 shows the amplified laser beam spectra after the tapered amplifier as function of its current. Figure 10(a) shows the seed spectrum. Figures 10 (b), (c), (d) and (e) show the spectra at 800 mA, 900mA, 1000 mA and 1100 mA respectively. Clearly, the optical power increases with the TA current (Fig. 11). Although the cutoff frequency does not vary with current (red dashed line in Fig. 10), the lower frequencies depend on the TA current. At maximum current, the tapered amplifier presents its own feedback in the spectrum (Fig. 10(e)). This can be avoided by operating it at lower currents. An alternative to address this issue would be to use a volumetric Bragg grating (VBG) [21] in the first pass through the TA to filter out the undesired frequencies, preventing them from being amplified in the second pass through the TA.

It is important to emphasize that, in this work, we focused exclusively on cutting the spectra very precisely at different frequencies, as this is crucial for molecular cooling applications, where shaping at a well-defined frequency is required [13]. Demonstrating advanced spectral shaping functions, such as band-pass filtering, notch filtering, or shaping over non-contiguous frequency domains, would be of interest for future studies targeting other applications.

OPTICS CONTINUUM

4. Conclusion

In this work, we built a spectral shaping system, based on a VIPA and a DMD, to manipulate a multimode diode laser spectrum. Its output was seeded, using a double-pass configuration, in a tapered amplifier. We have characterized the optical properties of the entire system with both a narrow-linewidth single-mode laser and a broadband multimode laser. The system resolution with the narrow-linewidth laser was 0.02 cm^{-1}. On the other hand, the resolution of the system with the multimode laser was 0.1 cm^{-1}, as our measurement was limited by the resolution of the spectrometer used. It is expected that the resolution with the multimode laser would be better than 0.1 cm^{-1}, but not as good as that achieved with the single-frequency laser, since the beam quality of the multimode laser is worse than that of the single-frequency laser. Eventually, the molecular rovibrational cooling signal could be used to manipulate the spectrum even with higher resolution.

Multimode diode lasers are relatively inexpensive devices, available for many wavelengths, and can also be temperature tuned. Therefore, such a system could easily be available to more researchers in different fields at different wavelengths, leading to more applications. The relatively low power (~ 60 mW) may be overcome by seeding a more powerful TA or slaving a multimode diode laser [22]. In our case, we plan to use it for the rovibrational cooling of Rb_2 molecules, whose rotational constant of the ground potential $X^1\Sigma_g^+$ is around ~0.022 cm^{-1} [13]. It might also be useful for other molecules such as SrBr and SrI [23,24].

Funding. Fundação de Amparo à Pesquisa do Estado de São Paulo (2018/06835-0, 2019/10971-0, 2021/04107-0, 2022/16904-5, 2023/06732-5); Conselho Nacional de Desenvolvimento Científico e Tecnológico (305257/2022-6); Agence Nationale de la Recherche (ANR-21-CE30-0060-01); Air Force Office of Scientific Research (FA9550-23-1-0666).

Acknowledgement. This work is supported by grants 2018/06835-0, 2019/10971-0, 2021/04107-0, 2022/16904-5 and 2023/06732-5, São Paulo Research Foundation (FAPESP), CNPq (305257/2022-6) and ANR-21-CE30-0060-01 (COCOTRAMOS project) from Agence Nationale de la Recherche. It is also supported by the US Air Force Office of Scientific Research (Grant FA9550-23-1-0666).

Disclosures. The authors declare no conflicts of interest.

Data availability. The experimental data are available from the authors upon reasonable request.

References

1. A. L. Schawlow, "Laser spectroscopy of atoms and molecules," Science **202**(4364), 141–147 (1978).
2. A. Marian, M. C. Stowe, J. R. Lawall, *et al.*, "United time-frequency spectroscopy for dynamics and global structure," Science **306**(5704), 2063–2068 (2004).
3. M. J. Thorpe, K. D. Moll, R. J. Jones, *et al.*, "Broadband cavity ringdown spectroscopy for sensitive and rapid molecular detection," Science **311**(5767), 1595–1599 (2006).
4. H. F. Passagem, R. Colín-Rodríguez, J. Tallant, *et al.*, "Continuous loading of ultracold ground-state $^{85}rb_2$ molecules in a dipole trap using a single light beam," Phys. Rev. Lett. **122**(12), 123401 (2019).
5. M. Cashen, V. Bretin, and H. Metcalf, "Optical pumping in 4he* with frequency-shifted feedback amplification of light," J. Opt. Soc. Am. B **17**(4), 530–533 (2000).
6. A. Bayerle, S. Tzanova, P. Vlaar, *et al.*, "Tapered amplifier laser with frequency-shifted feedback," SciPost Phys. **1**(1), 002 (2016).
7. M. Viteau, A. Chotia, M. Allegrini, *et al.*, "Optical pumping and vibrational cooling of molecules," Science **321**(5886), 232–234 (2008).
8. I. Manai, R. Horchani, H. Lignier, *et al.*, "Rovibrational cooling of molecules by optical pumping," Phys. Rev. Lett. **109**(18), 183001 (2012).
9. T. Courageux, A. Cournol, D. Comparat, *et al.*, "Efficient rotational cooling of a cold beam of barium monofluoride," New J. Phys. **24**(2), 025007 (2022).
10. A. Cournol, P. Pillet, H. Lignier, *et al.*, "Rovibrational optical pumping of a molecular beam," Phys. Rev. A **97**(3), 031401 (2018).
11. M. Shirasaki, "Large angular dispersion by a virtually imaged phased array and its application to a wavelength demultiplexer," Opt. Lett. **21**(5), 366–368 (1996).
12. S. Xiao, A. Weiner, and C. Lin, "A dispersion law for virtually imaged phased-array spectral dispersers based on paraxial wave theory," IEEE J. Quantum Electron. **40**(4), 420–426 (2004).
13. M. A. L. Torres, H. F. Passagem, D. R. Fernández, *et al.*, "Proposal for zeeman slowing of rb2 molecules in a supersonic beam, inducing internal cooling," J. Phys. B: At., Mol. Opt. Phys. **56**(6), 065301 (2023).

OPTICS CONTINUUM

14. V. Supradeepa, C.-B. Huang, D. E. Leaird, *et al.*, "Femtosecond pulse shaping in two dimensions: Towards higher complexity optical waveforms," Opt. Express **16**(16), 11878–11887 (2008).
15. V. R. Supradeepa, E. Hamidi, D. E. Leaird, *et al.*, "New aspects of temporal dispersion in high-resolution fourier pulse shaping: a quantitative description with virtually imaged phased array pulse shapers," J. Opt. Soc. Am. B **27**(9), 1833–1844 (2010).
16. S. A. Diddams, L. Hollberg, and V. Mbele, "Molecular fingerprinting with the resolved modes of a femtosecond laser frequency comb," Nature **445**(7128), 627–630 (2007).
17. S. Xiao and A. M. Weiner, "2-d wavelength demultiplexer with potential for ≥ 1000 channels in the c-band," Opt. Express **12**(13), 2895–2902 (2004).
18. S. X. Wang, S. Xiao, and A. M. Weiner, "Broadband, high spectral resolution 2-d wavelength-parallel polarimeter for dense wdm systems," Opt. Express **13**(23), 9374–9380 (2005).
19. A. J. Metcalf, V. Torres-Company, V. Supradeepa, *et al.*, "Fully programmable two-dimensional pulse shaper for broadband line-by-line amplitude and phase control," Opt. Express **21**(23), 28029–28039 (2013).
20. V. Bolpasi and W. V. Klitzing, "Double-pass tapered amplifier diode laser with an output power of 1 w for an injection power of only 200 uw," Rev. Sci. Instrum. **81**(11), 113108 (2010).
21. B. L. Volodin, S. V. Dolgy, E. D. Melnik, *et al.*, "Wavelength stabilization and spectrum narrowing of high-power multimode laser diodes and arrays by use of volume bragg gratings," Opt. Lett. **29**(16), 1891–1893 (2004).
22. C. J. H. Pagett, P. H. Moriya, R. Celistrino Teixeira, *et al.*, "Injection locking of a low cost high power laser diode at 461 nm," Rev. Sci. Instrum. **87**(5), 53105–53109 (2016).
23. L. Liu, C.-L. Yang, M.-S. Wang, *et al.*, "The spectroscopic properties of the low-lying excited states and laser cooling scheme of SrBr molecule," Spectrochimica Acta Part A: Mol. Biomol. Spectrosc. **228**, 117721 (2020).
24. L. Liu, C.-L. Yang, M.-S. Wang, *et al.*, "Spectroscopic properties of the low-lying electronic states and laser cooling feasibility for the SrI molecule," Chin. J. Phys. **71**, 435–443 (2021).